



Manizhe Zakeri*
Assistant Professor

Mehdi Kharazmi†
M.Sc.

Javad Faraji‡
Postdoc. Researcher

Low-dimensional Friction Modelling with Considering Random Asperity Distributions

This paper presents a new model to study the friction between rough surfaces with random distribution of the asperities, taking into account the contact mechanics. The results obtained show that as the surface separation decreases, the normal and friction forces increase and the coefficient of friction decreases. This model predicts higher friction forces and coefficient of friction than the model based on the Hertzian contact model. The sensitivity of the coefficient of friction to material properties is investigated using two sets of material properties. Assuming that the standard deviation and the radius of the asperities are constant, the first set investigates the variation of the adhesion energy, length of Burgers vectors, and elastic modulus parameters for the base material silicon. In the second set, real materials such as silicon, Fe, Cu, Au, and Ag are studied in contact with a silicon substrate. The results show that the friction coefficient decreases with the increase of the adhesion energy and increases with the increase of the length of Burgers vectors and elastic modulus.

Keywords: Nano scale Friction, Roughness, Contact Mechanics, Asperity Peak, Adhesion Energy

1 Introduction

1.1 Motivation

Friction parameters at the macro scale have significant effects, such as energy losses in rotating devices [1], loss of extrusion force [2]. The importance of friction has been highlighted in recent advances in nanotechnology and micro/nano-electromechanical systems (MEMS /NEMS), e.g., in the development of controls for micro/nano devices [3, 4] and the effects of vortex currents between particles and fluid [5].

* Corresponding Author, Assistant Professor, Faculty of Mechanical Engineering, University of Tabriz, 29 Bahman, Tabriz, Iran, m.zakeri@tabrizu.ac.ir

† M.Sc., Faculty of Mechanical Engineering, University of Tabriz, 29 Bahman, Tabriz, Iran, mehdi.kharazmi66@gmail.com

‡ Postdoctoral Researcher, Faculty of Mechanical Engineering, University of Tabriz, 29 Bahman, Tabriz, Iran, j.faraji@tabrizu.ac.ir

Friction is a force that resists the relative motion of two objects in contact.

Many aspects of friction are unknown, and tribology is the science that studies these unknowns. At the micro/nanoscale, accurate friction and contact models are required to accurately model the friction phenomena between contacting rough surfaces. To this end, the normal and frictional forces between contacted smooth surfaces must be studied for the desired rough surfaces [6-8].

1.2 Related literature

Recent advances in laboratory tools such as atomic force microscopy (AFM) have made it possible to measure the adhesion and friction properties of various surfaces at the atomic and molecular levels [9]. The coefficient of friction has a different value at the micro/nanoscale than at the macroscale, indicating the scale-dependent nature of the coefficient of friction. Many researchers have studied the effects of scale on friction [10-12]. The simplest proposed model is the modified Coulomb friction model, which is a popular model for research due to its simplicity [13, 14]. The friction model of Hurtado and Kim (HK) is a commonly used and precise friction model at the micro and nanoscale. It directly provides the necessary frictional stresses to accurately calculate the frictional forces, so that the friction stress is proportional to the contact radius [15, 16]. In the contact between two objects, contact mechanics is the main issue. The first model to study the normal forces at the interface between two contacting elastic objects was proposed by Hertz [14]. Johnson et al. studied contact mechanics at the micro/nanoscale considering short-range surface forces (JKR model) assuming elastic deformation [14]. Derjaguin et al. proposed a model to investigate long-range surface forces (DMT model) ignoring deformations [17]. A more comprehensive model was proposed by Maugis using the Dugdale's potential function (MD model) [18]. Assuming both short- and long-range surface forces, Schwarz proposed a general analytical model for adhesive elastic contact within certain ranges of the JKR and DMT models [19]. The models of MD and Schwarz include all areas of contact zones. However, due to the complexity of the models and the importance of elastic surface deformations at the nanoscale, the Hertz and JKR contact models are more commonly used to simplify contact mechanics and are suitable for nanoscale research [20-22]. Many studies have been performed to model the friction between two surfaces and to investigate the contact normal force and friction coefficient between rough surfaces [23-26]. The roughness of a surface changes the normal force and the contact area at the interface of the contacted surfaces on a micro/nanoscale.

Many researchers have modeled the friction of rough surfaces by considering the distribution of asperities and the different profiles of a rough surface [27-29]. One method for defining the profiles of rough surfaces is the Greenwood-Williamson (GW) roughness model, which uses the Gaussian probability distribution function to model the distribution of the asperity height. Adams et al. (AM) proposed a complex contact model that combines the Hertz and MD models with the friction and roughness model [18, 30]. Due to the MD contact model does not use continuous equations in problems with complex interactions, the calculation of the contact area with this model is very complicated. On the other hand, the indentation depth obtained from the contact model should be used in the equations of the GW roughness model and HK friction model. Therefore, the theories based on MD do not properly consider the indentation depth in the GW model and the HK friction model. Therefore, a model that compensates for the weaknesses of the methods under study is urgently needed.

1.3 Contribution

Considering the theory of continuum mechanics and its effectiveness in predicting friction behavior, this paper models and investigates the friction behavior of rough surfaces based on

JKR's contact model. In this work, a developed AM (DAM) model is proposed to accurately study the frictional behavior of rough surfaces at the nanoscale. DAM is extracted by combining the analytical JKR contact model with the GW roughness distribution, and HK friction models, and the results are compared with those obtained based on the Hertz, DMT, and Schwartz contact models. Although the peak radius of the asperities is the same in GW theory, the contact radii are different when the height of the asperities at the contact point of the two surfaces is considered; therefore, the changes in the contact area have been taken into account in this paper. In other words, the contact radius is determined based on the indentation depth and the height of the asperities, and then the contact forces are calculated. Finally, the effects of the parameters of the rough surface, including the standard deviation of the height of the asperity and the peak radius of the asperity, and the parameters of the surface material, including the elastic modulus, the adhesion energy, and the length of the Burgers, length on the frictional behavior of the rough surfaces are investigated. In particular, these analyzes show the pure effects of the surface roughness parameters and the material parameters on the frictional behavior.

This will contribute to an accurate prediction of the frictional behavior under different conditions. The structure of the paper is as follows. The second section discusses the GW roughness distribution model, the HK friction model, and the contact mechanics models, including Hertz, JKR, DMT, and Schwarz. The rest of this section deals with the combination of the aforementioned methods to obtain the final equations of the presented model. The third section deals with the simulation. Finally, the conclusion is presented.

2 Modeling the friction between surfaces with random asperity distributions

In the following, the theories required to study friction between surfaces with random roughness are examined, including the GW roughness distribution model, the HK friction model, and contact models such as Hertz, JKR, DMT, and Schwarz. Finally, a complete model for studying friction between surfaces with random roughness is proposed.

2.1 GW roughness distribution model

To study the normal forces between two rough surfaces, the GW model is proposed, which uses a Gaussian probability distribution function to distribute the roughness height [13]. This distribution function uses surface properties such as the standard deviation of the roughness height and the radius of the peaks of the asperities. The basic assumptions of the GW model used in this study are [25]:

1. The rough surface is isotropic.
2. The roughness has the shape of a dented sphere.
3. All the asperities have the same radius of curvature and the height of the asperities changes randomly.
4. There is no volumetric and interventional interaction between adjacent asperities.

Figure (1) shows the general scheme of contact between a flat surface and a rough surface with a random distribution of asperities. The parameter d indicates the distance between the mean surface height of the substrate and the surface of the top, and δ is the indentation depth of the two objects, which is equal to $z - d$. The height of the asperity relative to the mean surface height of the substrate is denoted by z . The probability of an asperity height to be between the values z and $z + dz$ can be calculated by $\varphi(z)dz$, where $\varphi(z)$ is the probability function for the height of asperities on rough surfaces. The sum of the probabilities for the in contact asperities of surfaces that are in distance d apart, is expressed as follows [25]:

$$\text{prob}(z > d) = \int_d^{\infty} \varphi(z)dz \quad (1)$$

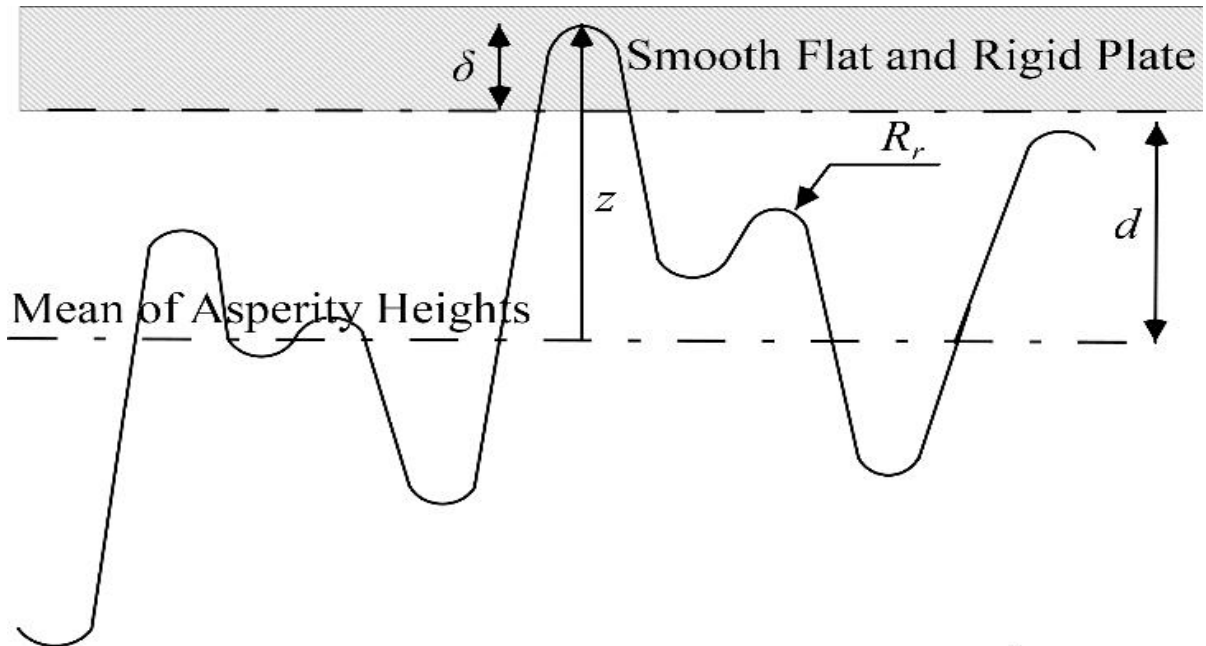


Figure 1 Schematic of the contact between a smooth surface and a rough surface with a random distribution

The number of asperities in contact, n , is calculated by Eq. (2) [10]:

$$n = N \int_a^{\infty} \varphi(z) dz \quad (2)$$

where N is the nominal number of surface asperities.

In the GW model, the probability roughness function is defined using the Gaussian probability distribution function as follows:

$$\varphi(z) = \frac{1}{\sigma\sqrt{2\pi}} e^{-\frac{(z-\mu)^2}{2\sigma^2}} \quad (3)$$

where μ and σ are the average height of the asperities and the standard deviation of the asperity height, respectively.

2.2 Friction models

Several models have been proposed to measure friction between surfaces, but only the modified Coulomb friction model and the HK friction models use the contact area between two objects to determine the friction force. The stress-dependent HK friction model is a micromechanical model for predicting the sliding friction force between two asperities peaks for different contact radii [15, 30].

This model creates a set of dimensionless parameters to study the elastic and plastic deformations of the asperities peaks as a function of shear stress. Figure (2) shows the dimensionless frictional stress ($\bar{\tau}_f$) as a function of the dimensionless contact radius (\bar{a}). According to Fig. (2) in the HK model, the shear stress has the highest value when the dimensionless contact radius is smaller than an initial critical value. As the dimensionless contact radius increases, the shear stress decreases (part 2) until it reaches the second constant value (part 3). The left and right limits in Fig. (2) are $(\bar{a}_1, \bar{\tau}_{f1})$ and $(\bar{a}_2, \bar{\tau}_{f2})$, respectively, and correspond to $(28, \frac{1}{43})$ and $(8000, \frac{\bar{\tau}_{f1}}{30})$ [30].

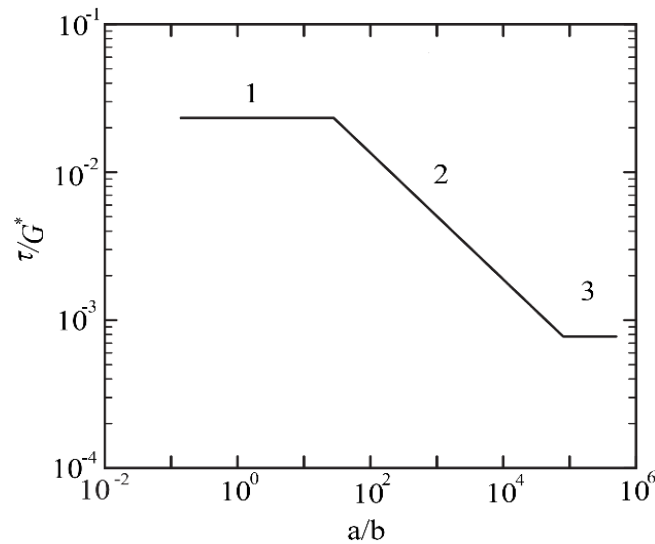


Figure 2 Relation between dimensionless friction stress dimensionless contact radius according to HK model [25]

The dimensionless frictional stress and the dimensionless contact radius are obtained from Eqs. (4) and (5) [30]:

$$\bar{\tau}_f = \frac{\tau_f}{G^*} \tag{4}$$

$$\bar{a} = \frac{a}{b} \tag{5}$$

where a is the contact radius, b is the length of the Burgers vector, τ_f is the friction stress, and G^* is the effective shear modulus.

The effective shear modulus for two objects in contact is calculated as follows:

$$G^* = \frac{2G_1G_2}{(G_1+G_2)} \tag{6}$$

The values of $\bar{\tau}_f$ obtain as:

$$\log(\bar{\tau}_f) = \begin{cases} \log(\bar{\tau}_{f1}) & \bar{a} < \bar{a}_1 \\ M\log(\bar{a}) + B & \bar{a}_1 < \bar{a} < \bar{a}_2 \\ \log(\bar{\tau}_{f2}) & \bar{a}_2 < \bar{a} \end{cases} \tag{7}$$

where M and B are expressed by Eqs. (8) and (9), respectively [25]:

$$M = -\frac{\log(\frac{\bar{\tau}_{f1}}{\bar{\tau}_{f2}})}{\log(\frac{\bar{a}_2}{\bar{a}_1})} \tag{8}$$

$$B = \frac{\log(\bar{\tau}_{f1})\log(\bar{a}_2) - \log(\bar{\tau}_{f2})\log(\bar{a}_1)}{\log(\bar{a}_2/\bar{a}_1)} \tag{9}$$

The friction force for each asperity peak is determined as follows [25]:

$$F_f = \pi a^2 \tau_f \quad (10)$$

By integrating the friction force F_f and the GW model, the final value of the friction force between rough surfaces is given as Eq. (11). It is obtained by adding the friction forces acting on the n peaks of the asperities.

$$F_{f\text{total}} = N \int_a^\infty F_f(z) \varphi(z) dz \quad (11)$$

In addition, if the upper surface is smooth, the dimensionless friction force according to the HK friction model will be obtained by Eq. (12) [14]:

$$\begin{aligned} \bar{F}_{f\text{total}} = \frac{F_{f\text{total}}}{NGb^2} = & 2\pi \int_{\bar{z}_2}^\infty \bar{\tau}_{f2} \bar{a}^2 \varphi(\bar{z}) d\bar{z} + 2\pi \int_{\bar{d}}^{\bar{z}_1} \bar{\tau}_{f1} \bar{a}^2 \varphi(\bar{z}) d\bar{z} + \\ & 2\pi \int_{\bar{z}_1}^{\bar{z}_2} 10^B \bar{a}^{M+2} \varphi(\bar{z}) d\bar{z} \end{aligned} \quad (12)$$

2.3 Contact mechanics

This section presents the necessary details of the models used in this investigation, including those of Hertz, JKR, DMT, and Schwarz.

2.3.1 Hertz model

The normal force between two spherical surfaces in the Hertz model is calculated by Eq. (13). Considering the contact of rough surfaces, the Hertz force is applied to each contacted asperity [14].

$$P = \frac{4}{3} E^* R_s^{\frac{1}{2}} \delta^{\frac{3}{2}} \quad (13)$$

where E^* and R_s are the effective Young's modulus and the effective radius of the contacted surfaces defined by Eqs. (14) and (15), respectively [14]:

$$E^* = \left(\frac{1-\nu_1^2}{E_1} + \frac{1-\nu_2^2}{E_2} \right)^{-1} \quad (14)$$

$$R_s = \frac{R_1 R_2}{R_1 + R_2} \quad (15)$$

In the Hertz model, the indentation depth δ is expressed as follows [14]:

$$\delta = \frac{a^2}{R_s} \quad (16)$$

2.3.2 JKR model

According to the JKR contact model, the normal force between two spherical surfaces is calculated by Eq. (17). Considering the contact of rough surfaces, the JKR force is applied to each contacted asperity [14]:

$$P_{JKR} = (P + 3\gamma\pi R_s + \sqrt{6\gamma\pi R_s P + (3\gamma\pi R_s)^2}) \quad (17)$$

where P is the external force applied between the two objects in contact, and P_{JKR} is the total normal force in the presence of the short-range surface forces. γ is the adhesion energy, indicating the amount of energy per unit area ($\frac{J}{m^2}$) required to separate the surfaces. It is measured based on the material of the surfaces that are in contact (Eq. (18)) [31].

$$\gamma = \gamma_1 + \gamma_2 - \gamma_{12} \quad (18)$$

The contact radius and indentation depth of the JKR model are obtained from Eqs. (19) and (20), respectively [14].

$$a_{JKR} = \left(\frac{3R_s}{4E^*} P_{JKR}\right)^{\frac{1}{3}} \quad (19)$$

$$\delta = \frac{a_{JKR}^2}{R_s} - \sqrt{\frac{2\pi\gamma a_{JKR}}{E^*}} \quad (20)$$

2.3.3 DMT model

The normal force for a single asperity peak in the DMT contact model is calculated as follows [14]:

$$P_{DMT} = (P + 2\gamma\pi R_s) \quad (21)$$

where P_{DMT} is the normal force in the presence of the long-range surface forces. As indicated in Eqs. (22) and (23), the radius and indentation depth in this model are similar to those in the Hertz equation [18].

$$\delta = \frac{a_{DMT}^2}{R_s} \quad (22)$$

$$a_{DMT} = \left(\frac{R_s}{E^*} (P + 2\pi\gamma R_s)\right)^{\frac{1}{3}} \quad (23)$$

2.3.4 Schwarz model

The Schwarz model assumes that the interaction between the surfaces is similar to the JKR model and that the long-range forces are added as an external force. To obtain the relationship between the contact radius and the applied load, the extraction method of the JKR model is used. Considering the normal force of the JKR model as the equivalent Hertzian force P_H^{JKR} , Eq. (24) is obtained [18].

$$P_H^{JKR} = P + 3\pi R_s \gamma + \sqrt{6\pi R_s \gamma P + (3\pi R_s \gamma)^2} \quad (24)$$

By replacing the external force in Eq. (24) with the sum of the external force and long-range force ($P = P + 2\pi\gamma R_s$), the equivalent Hertzian force of the Schwarz model is obtained as follows:

$$P_H^{JKR} = P + 2\pi R_s \gamma_2 + 3\pi R_s \gamma_1 + \sqrt{6\pi R_s \gamma_1 (P + 2\pi R_s \gamma_2) + (3\pi R_s \gamma_1)^2} \quad (25)$$

The indentation depth and the contact radius are same as the JKR equations. The relation between the indentation depth and the contact radius is expressed by Eq. (26).

$$\delta = \frac{a^2}{R_s} - \tau_1 \sqrt{\frac{2\pi\gamma a}{E_s}} \quad (26)$$

2.4 Contact mechanics in rough surfaces

Now, the indentation depth δ equals to $z - d$ on the AM (Fig. (1)). Therefore, the total normal force (sum of the contact forces at peaks of the asperities) is defined by Eq. (27), which is obtained by substituting Eqs. (2) and (16) into Eq. (13) [30].

$$P_{total} = N \int_d^\infty P(z) \varphi(z) dz \quad (27)$$

For instance, normal force of Hertz model can be obtained from Eq. (28).

$$P = \frac{4}{3} E^* R_s^{\frac{1}{2}} N \int_d^\infty (z - d)^{\frac{3}{2}} \varphi(z) dz \quad (28)$$

In the method of GW model, the standard deviation of the height of the asperities σ is used to obtain the dimensionless variables such as the distance of the surfaces and the height of the asperities. In addition, two other dimensionless parameters are defined, α and β . The first parameter α represents the surface roughness, expressed by Eq. (29). The second parameter β denotes the ratio between the contact radius and the length of the Burgers vector for an indentation depth equal to the standard deviation of the Gaussian function defined by Eq. (30) [32]:

$$\alpha = \left(\frac{\sigma}{R_s}\right)^{\frac{1}{2}} \quad (29)$$

$$\beta = \frac{(R_s \sigma)^{\frac{1}{2}}}{b} \quad (30)$$

Finally, the dimensionless contact force of the Hertzian model is calculated as follows, where the upper surface is rigid, flat, and smooth:

$$\bar{P}_n = \frac{P}{\alpha N G_2 b^2} = \frac{4}{3} \frac{2}{1-\nu_2} \beta^2 \int_{\bar{d}}^{\infty} (\bar{z} - \bar{d})^3 \varphi(\bar{z}) d\bar{z} \quad (31)$$

The equivalent coefficient of friction for contact between a flat, smooth surface and a randomly rough surface with a Gaussian distribution function is given by Coulomb's law as follows:

$$\alpha \mu_s = \frac{\bar{F}_{\text{friction}}}{\bar{P}_n} \quad (32)$$

The same method is used for other contact models. The normal and frictional forces are calculated using Eqs. (29) and (11). Therefore, the coefficient of friction is obtained as follows:

$$\mu_s = \frac{F_{\text{friction}}}{P} \quad (33)$$

3 Simulation and discussion

This section deals with the simulation and study of the frictional behavior of contacting surfaces by determining the friction variables, including the normal force, the frictional force, and the coefficient of friction. In the following, the frictional behavior of smooth and rough surfaces in contact is first investigated by applying the proposed model using the JKR, DMT, and Schwarz contact models. In addition, the effects of changes in roughness parameters, including standard deviation of asperity height and radius of asperities peaks, and changes in material properties, including adhesion energy, length of Burgers vector, and elastic modulus, investigate. In the friction behavior simulation, the contact area material is assumed to be silicon and its physical properties are defined in Table (1). The value of γ , the equivalent adhesion energy between two silicon surfaces, is equal to 0.2 j/m^2 [31]. The mean, standard deviation of the height of the asperities and the radius of the peaks of the asperities are assumed to be 0, 1 and 50 *nm*, respectively.

The range of variation in the parameters of rough surfaces largely corresponds to that of real surfaces [21, 34]. Therefore, from previous experimental results on surface roughness use to obtain the values for the standard deviation of the asperity height and the radii of the asperity peaks [23, 25]. The numbers of asperities that are in contact with the upper surface obtain by using the Gaussian probability distribution function. Hence, the number of contacted asperities changes due to variation of the surface separation. At any moment, the smooth surface is in contact with at least one asperity of the rough surface. Depending on the distance between the in-contact surfaces, the effective contact radius and the standard deviation of asperity height, and the probability of the in-contact asperity varies and the contact area obtain by using the number of contacted asperities, instantaneously. Therefore, the normal and friction forces have been calculated considering the obtained contact area at different values of the distance. The normal force, friction force, and friction coefficient are calculated analytically by simultaneously solving all equations containing the GW roughness distribution, contact mechanics, and friction model equations.

Table 1 Physical characteristics of the silicon surface [32, 33].

$E(\text{GPa})$	$G(\text{GPa})$	ν	$\rho(\text{kg/m}^3)$	$b(\text{nm})$
169	66.54	0.27	2330	0.191

The accuracy of the generated results has been verified by comparing with the existing results of AM [25, 30] in Figs. (3) to (6). The diagram of the scaled friction coefficient as a function of the dimensionless normal force, based on AM, is shown in Fig. (3). It shows the changes in the scaled coefficient of friction for different values of β (the ratio of the contact radius to the length of the Burgers vector), based on Eq. (32). It can be observed that the coefficient of friction decreases as the value of β increases. Moreover, the slope of the friction coefficient curve becomes steeper for smaller values of β . Note that according to the HK friction model, the frictional stress is larger for smaller contact radii. Therefore, the coefficient of friction exhibits significant changes for smaller values of β . For higher values of β , the friction coefficient is almost constant and almost independent of the dimensionless normal force. The results shown in Fig. (3) have been verified and are similar to those of previous results [13, 30]. In the following, the frictional behavior of the surfaces is investigated using the JKR contact model. Due to the complexity of the dimensionless models, the dimension values of the AM results are used to allow comparison of the obtained results with the AM.

The obtained results are shown in Figs. (4) to (9) and verified by comparison with AM. In addition, the effects of the roughness parameters, including the standard deviation of asperity height σ and the peak radius R_r of the asperity on the friction forces and the friction coefficient are investigated. In general, it is observed that as the distance increases, the normal and friction forces decrease. This is since the probability of contact between the asperities and the upper surface decreases. In addition, the DAM predicts higher normal and friction forces than AM. This is due to the inclusion of short-range adhesion forces in the JKR contact model. In addition, the difference between the forces calculated by AM and DAM increases as the distance decreases. This is because the short-range forces increase significantly at smaller distances compared to the external forces. The projected magnitudes of forces are elevated by as much as 20% compared to the values established through AM model when observing surface distances of less than 1 nm. Figures (4) and (5) show the changes in normal and frictional forces as a function of distance for different values of the standard deviation of the asperity height σ . As the standard deviation of asperity height increases, the normal and frictional forces also increase. This is due to the fact that for larger values of the standard deviation, the possibility of contact between the asperities and the upper surface increases, leading to an increase in the forces.

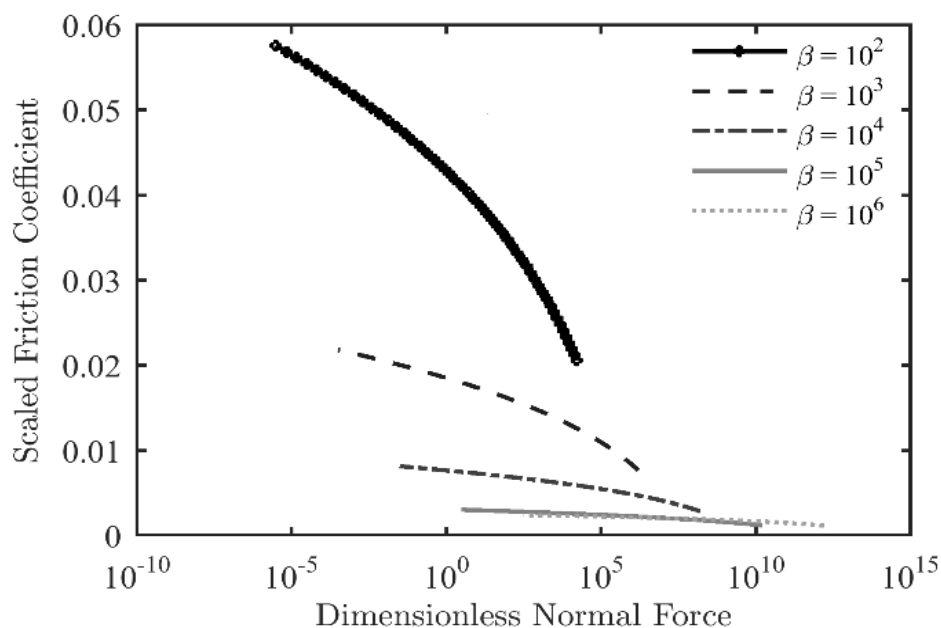


Figure 3 Scaled friction coefficient and dimensionless normal force without consideration of adhesion.

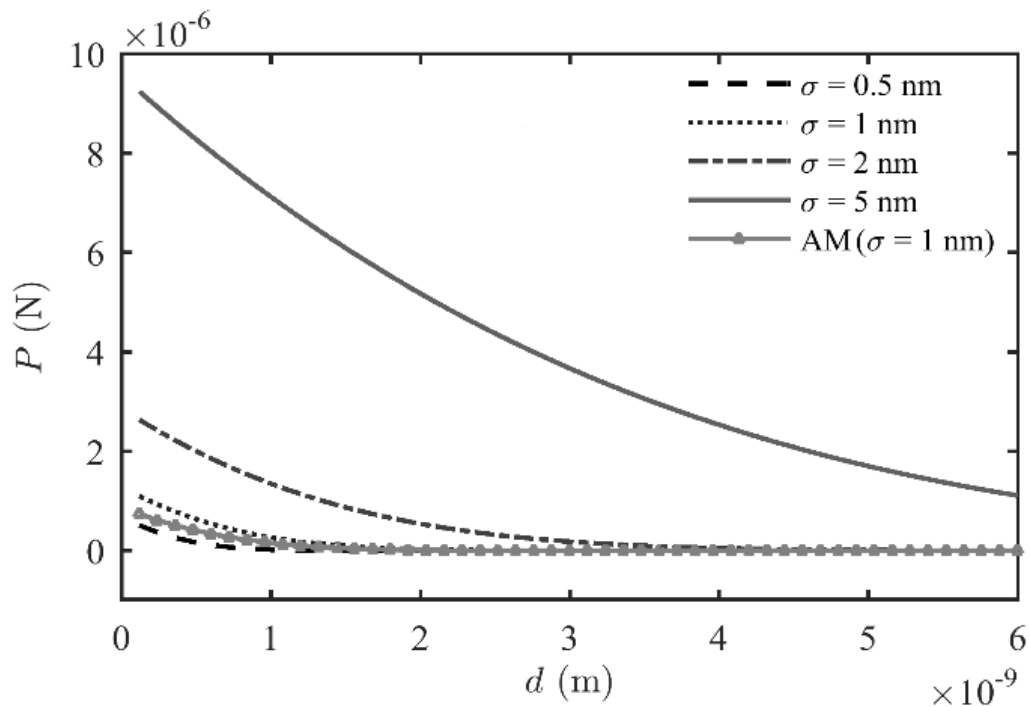


Figure 4 Comparison between the DAM and AM ($\sigma = 1 \text{ nm}$ and $R_r = 50 \text{ nm}$) and effect of standard deviations on normal force in the DAM ($R_r = 50 \text{ nm}$)

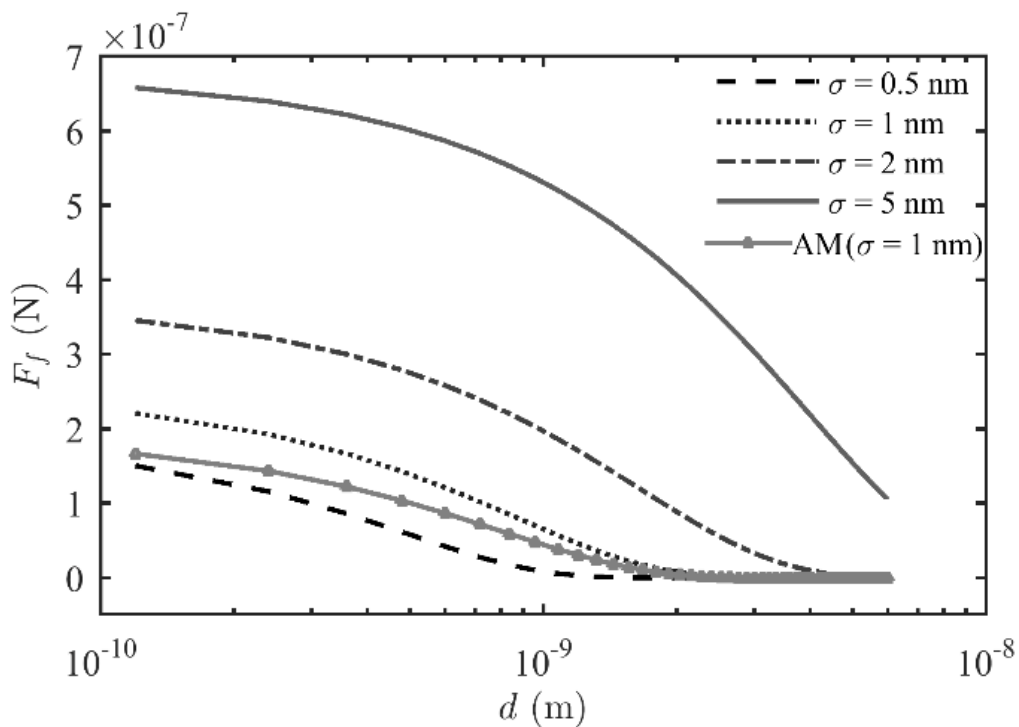


Figure 5 Comparison between the DAM and AM ($\sigma = 1 \text{ nm}$ and $R_r = 50 \text{ nm}$) and effect of standard deviations on friction force in the DAM ($R_r = 50 \text{ nm}$)

In Figs. (6) and (7), the effects of varying the peak radius of the asperities on the frictional behavior of the contact surfaces are investigated using the JKR contact model. When the radius of the asperity increases, both the normal and frictional forces increase. Increasing the radius of the asperity leads to larger contact areas between the asperities and the flat surface. Finally, the normal and frictional forces, which are directly related to the contact area, also increase.

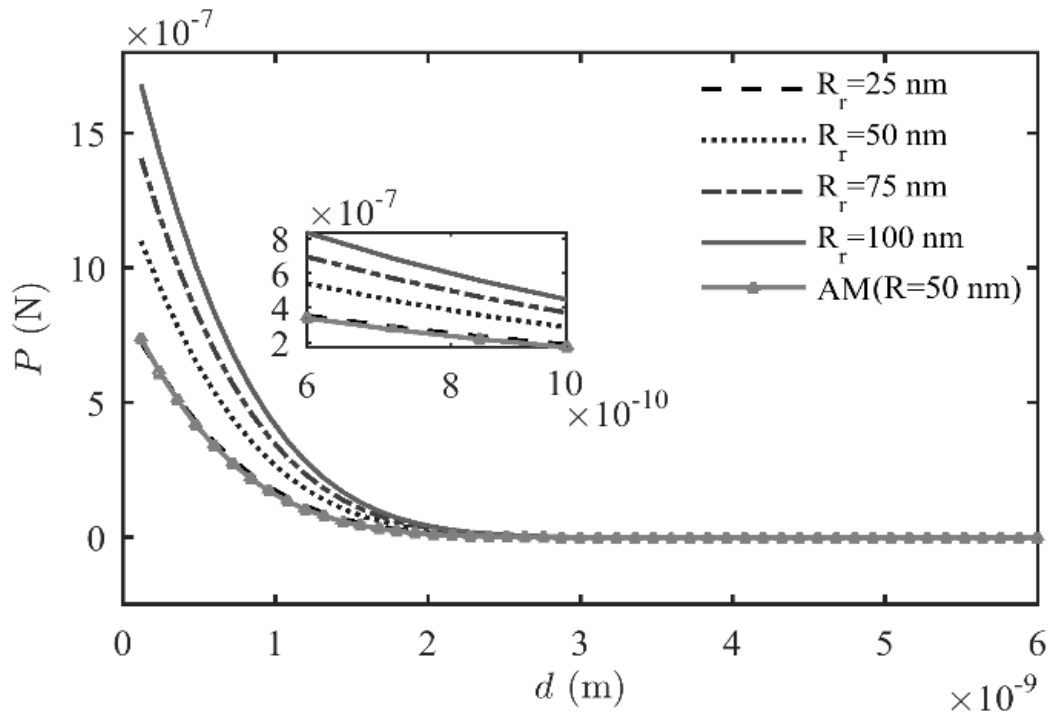


Figure 6 Comparison between the DAM and AM ($\sigma = 1 \text{ nm}$ and $R_r = 50 \text{ nm}$) and effect of asperity peak radii on normal force in the DAM ($\sigma = 1 \text{ nm}$)

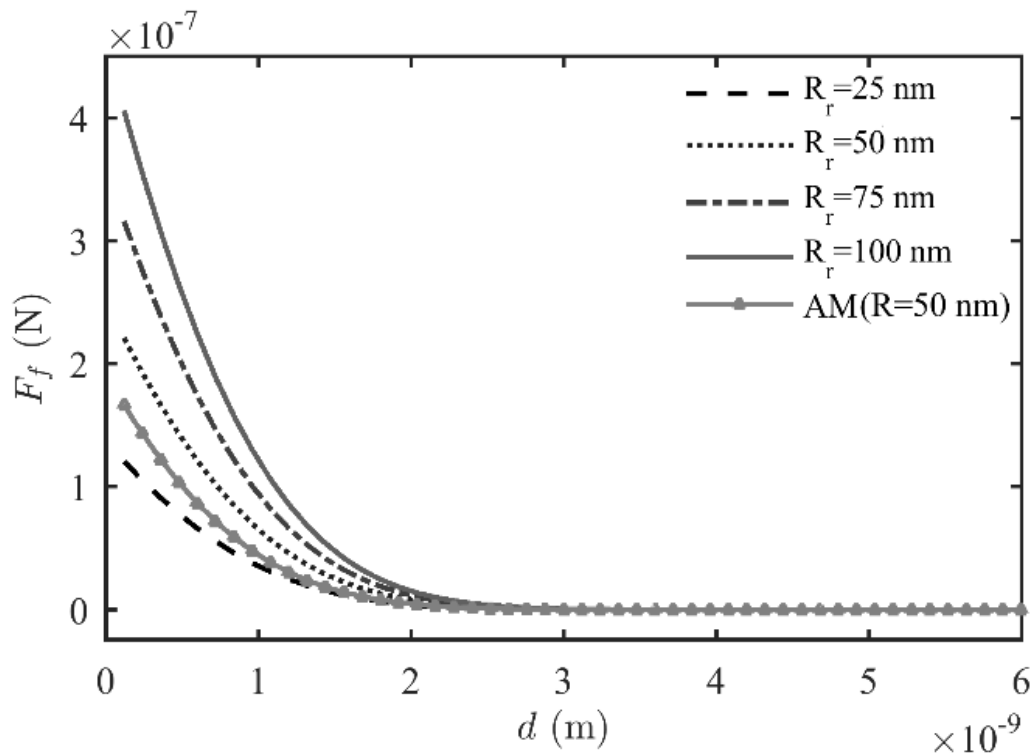


Figure 7 Comparison between the DAM and AM ($\sigma = 1 \text{ nm}$ and $R_r = 50 \text{ nm}$) and effect of asperity peak radii on friction force in the DAM ($\sigma = 1 \text{ nm}$)

Figures (8) and (9) show the effects of the roughness parameters, including the standard deviation of the asperity height σ and the peak radius R_r , on the coefficient of friction. Overall, the coefficient of friction decreases with increasing normal force. This downward trend is initially steeply increasing, but eventually approaches zero.

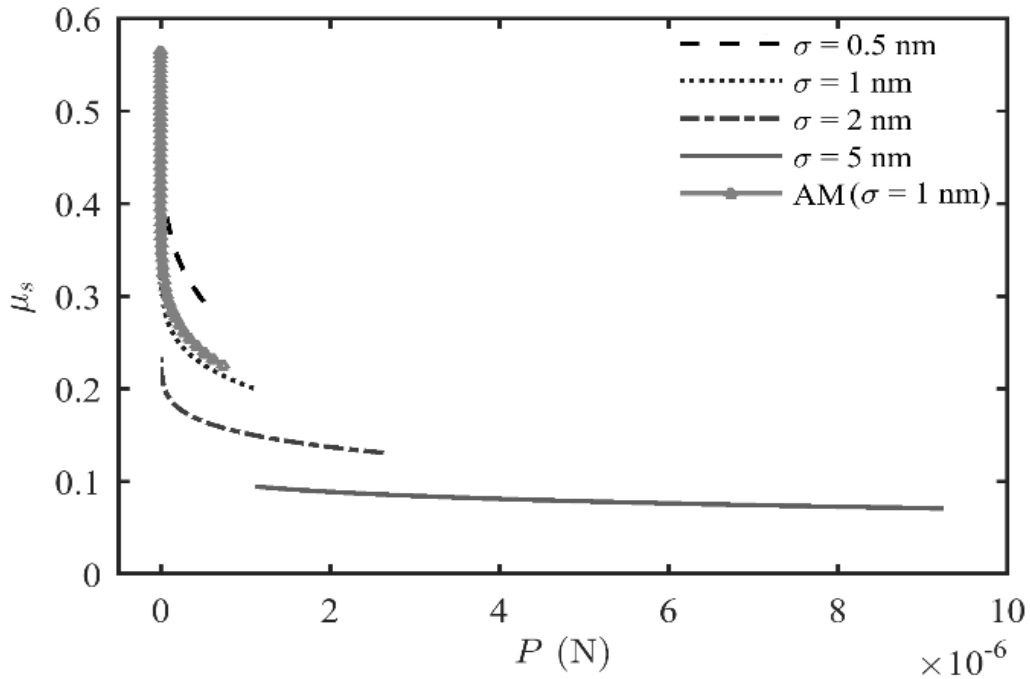


Figure 8 Comparison of friction coefficient between the DAM and AM ($\sigma = 1 \text{ nm}$ and $R_r = 50 \text{ nm}$), and effect of various standard deviation on friction coefficient in the DAM ($R_r = 50 \text{ nm}$)

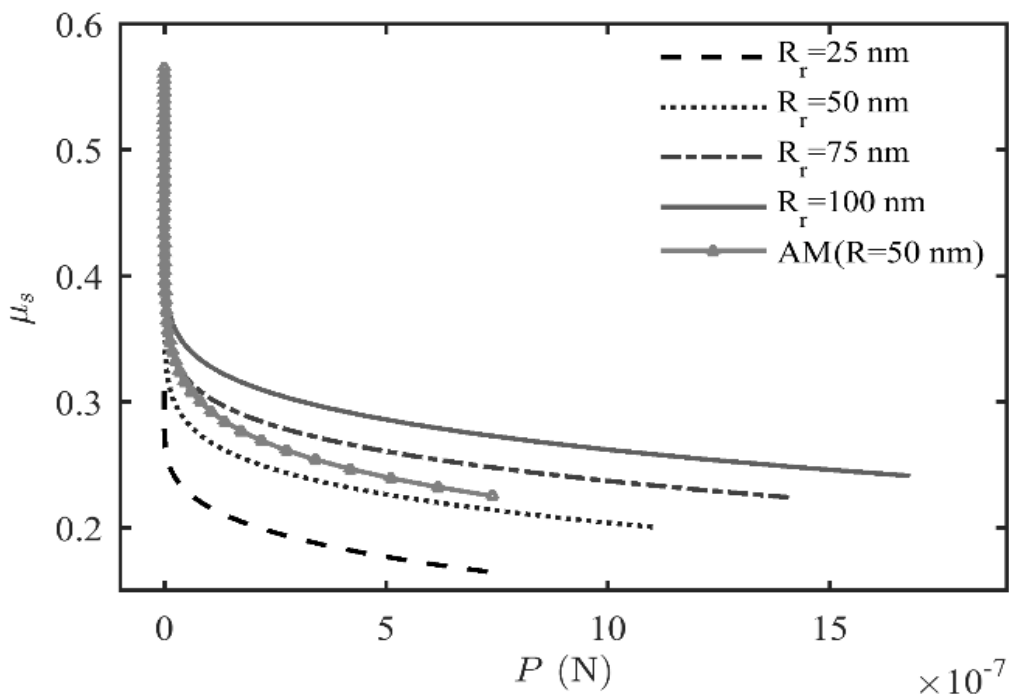


Figure 9 Comparison of friction coefficient between the DAM and AM ($\sigma = 1 \text{ nm}$ and $R_r = 50 \text{ nm}$), and effect of various asperity peak radii on friction coefficient in DAM ($\sigma = 1 \text{ nm}$)

Table 2 Physical properties of used materials [30, 35].

Material	$b(\text{nm})$	$E(\text{GPa})$	$\gamma(\text{j/m}^2)$	ϑ
Si	0.191	169	0.2	0.27
Fe	0.248	211	0.103	0.29
Cu	0.255	128	0.138	0.34
Au	0.284	79	0.222	0.44
Ag	0.288	83	0.197	0.37

This is due to the fact that the HK friction model predicts a larger frictional stress for a smaller contact radius than for a larger radius. In addition, the coefficient of friction obtained with the AM is lower than the results from DAM. This is the result of a larger increase in the normal force relative to the frictional force. On the other hand, it can be seen in Fig. (8) that the coefficient of friction decreases as the standard deviation of the height of the asperity increases. This decrease is particularly pronounced for smaller values of the standard deviation of the asperity height. As the standard deviation increases, the probability of contact between an asperity and the upper surface also increases, resulting in an increase in the contact area and a greater increase in the normal force than in the frictional force. As a result, the coefficient of friction decreases. Figure (9) shows that as the peak radius of the asperities increases, the coefficient of friction also increases. Assuming a constant normal force, as the peak radius of the asperities increases, the friction force between the upper smooth surface and the lower rough surface increases; consequently, the ratio between the friction force and the normal force increases, as does the coefficient of friction. The slope of this increase is less than the effect of the standard deviation of the asperity height. An increase in the coefficient of friction with smaller contact radii and larger normal force was also found in the study of Yu et al [27].

In Figs. (10) to (12), the sensitivity of the friction coefficient to the variation of material properties including the adhesion energy γ , the length of the Burgers vector b , and the elastic modulus E is investigated. It is assumed that the standard deviation of the height of the asperities and the peak radius of the asperities have constant values of 1 nm and 50 nm, respectively. In the simulations performed, the base material is silicon and the effect of the variation of a single parameter on the friction coefficient is studied assuming that the other parameters of the material are constant. If we also assume that all parameters change in real materials, we obtain the diagrams in Figs. (10) to (12), which show the changes in the coefficient of friction for real materials in contact with a silicon substrate. A list of the materials used and their physical properties can be found in Table (2), including Fe, Cu, Au and Ag.

For a detailed analysis of the effects of material properties, we have tried to select materials that have similar values in at least one of their main parameters. For example, the lengths of the Burgers vector of Fe and Cu or Au and Ag are very close. Au and Ag also have very similar elastic modulus values. In addition, the values of the adhesion energy of silicon, Au and Ag are close to each other. Based on the values given in Table (2), the properties of the different materials were compared in Eq. (34):

$$\begin{aligned} \gamma_{\text{Fe}} < \gamma_{\text{Cu}} < \gamma_{\text{Ag}} \cong \gamma_{\text{Si}} < \gamma_{\text{Au}} \\ E_{\text{Au}} < E_{\text{Ag}} < E_{\text{Cu}} < E_{\text{Si}} < E_{\text{Fe}} \\ b_{\text{Si}} < b_{\text{Cu}} \cong b_{\text{Fe}} < b_{\text{Au}} \cong b_{\text{Ag}} \end{aligned} \quad (34)$$

Figure (10) shows the change in the coefficient of friction versus the surface normal force for different values of the adhesion energy. The diagrams in Fig. (10) are divided into two groups. The first group of diagrams obtained for a base material of silicon and assuming a variation of the adhesion energy and constant values of the other parameters. The second group of diagrams have been obtained for the real materials. It can be seen in the silicon diagrams that the coefficient of friction decreases with increasing adhesion energy, which is consistent with the results of previous studies. In addition, as mentioned above, the changes in the coefficient of friction for real materials have been presented in the second set of diagrams by considering the changes in other material parameters. Considering Eq. (34), in which $\gamma_{\text{Fe}} < \gamma_{\text{Cu}} < \gamma_{\text{Ag}} \cong \gamma_{\text{Si}} < \gamma_{\text{Au}}$, and considering the results of previous researches, it is expected that the friction coefficient for Cu (which has a very low adhesion energy relative to silicon) to be much higher than that of silicon, and the friction coefficient for Ag (with an adhesion energy which is relatively lower

than or equal to that of silicon) to be greater than or equal to that of silicon. However, according to the obtained results, the friction coefficient of Cu is almost equal to that of silicon and the friction coefficient of Ag is much smaller than that of silicon. Moreover, the variations of friction coefficient with adhesion energy in the first set of diagrams is negligible, however, it is considerable in the second set of diagrams. These findings contradict the results of the previous research works and indicate the importance of other material parameters.

Figure (11) shows the change in the coefficient of friction versus the surface normal force for different values of the length of the Burgers vector. The values of the adhesion energy, the modulus of elasticity, the standard deviation of the height of the asperity and the peak radius of the asperity are considered constant.

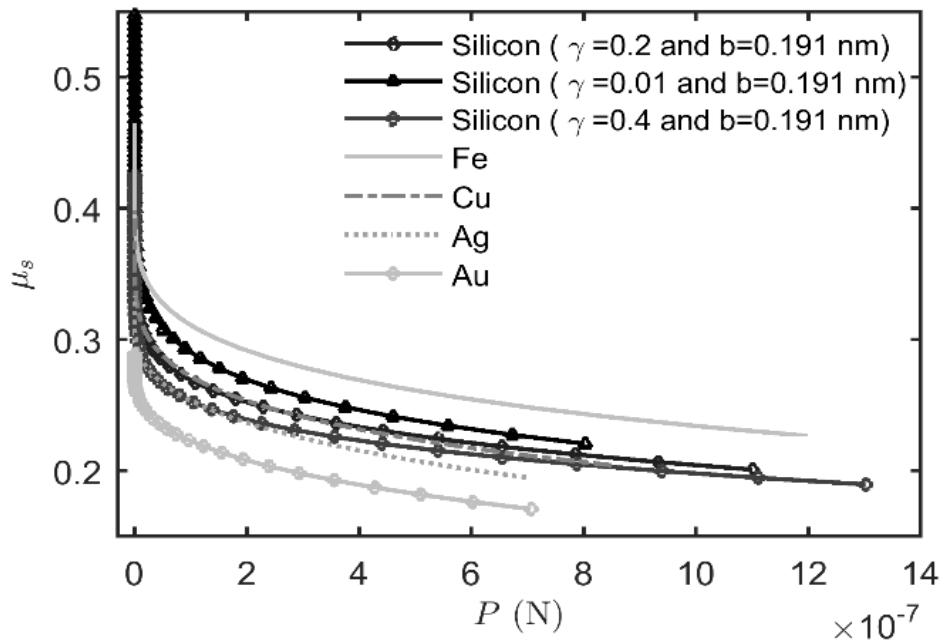


Figure 10 Effect of adhesion, Burgers vector and material type on friction coefficient ($\sigma = 1 \text{ nm}$ and $R_r = 50 \text{ nm}$)

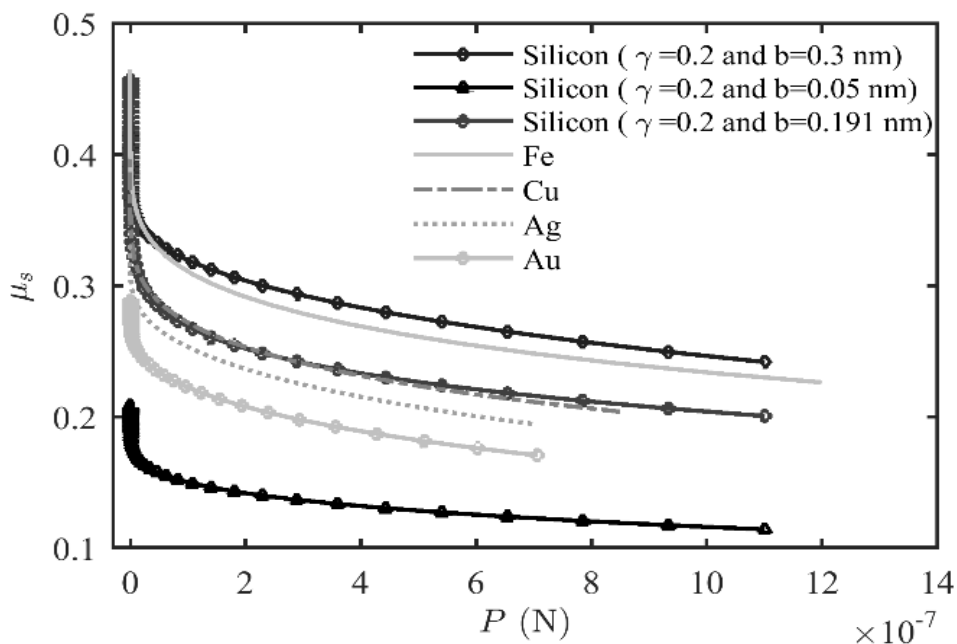


Figure 11 Effect of adhesion, Burgers vector and material type on friction coefficient ($\sigma = 1 \text{ nm}$ and $R_r = 50 \text{ nm}$)

It can be seen in the silicon diagrams that the coefficient of friction increases with increasing length of Burgers vector b , which is due to the increase in contact area at higher frictional stress. This result is consistent with the results of previous studies [6]. Taking into account the fact that the length of the Burgers vector actually depends on the type of material used, the changes in the coefficient of friction with the length of the Burgers vector are presented for real materials, also taking into account the changes in the other material parameters. Considering Eq. (34), in which $b_{Si} < b_{Cu} \cong b_{Fe} < b_{Au} \cong b_{Ag}$, and considering the results of previous research, it is expected that the friction coefficients of Au, Ag and Cu are higher than those of silicon, which have a greater length of the Burgers vector compared to silicon. However, according to the results obtained, these materials have a lower coefficient of friction than silicon, which emphasizes the importance of all parameters. Since a decrease in the elastic modulus reduces the frictional stress, increasing the length of the Burgers vector alone does not always increase the coefficient of friction; the effects of other parameters must also be taken into account.

Figure (12) shows the variation of the coefficient of friction with respect to the surface normal force for different values of the elastic modulus in the range (119-219 GPa). The values of the adhesion energy, the length of the Burgers vector, the standard deviation of the height of the asperities, and the peak radius of the asperities are considered constant. From Fig. (12) for silicon, it can be seen that the coefficient of friction increases as the elastic modulus increases which is also seen in [36]. This is because the increase in elastic modulus leads to an increase in shear modulus, thus increasing the frictional force. Furthermore, the changes in the coefficient of friction are plotted with the elastic modulus for real materials, taking into account the changes in other material parameters. Considering the diagrams of friction coefficients obtained for silicon-based material properties with a modified elastic modulus of 219 GPa and Fe with 211 GPa , it is expected that the friction coefficient of silicon (with a modified elastic modulus of 219 GPa) is higher than that of Fe. However, the obtained results show that the coefficient of friction of silicon is lower than that of Fe in this situation. Therefore, an increase in the elastic modulus E alone does not always lead to an increase in the coefficient of friction, but the effects of other parameters must also be taken into account.

So far, friction behavior has been studied using the JKR contact model. In the next step of this research, the effects of other contact models will be investigated by adding the DMT and Schwarz contact models.

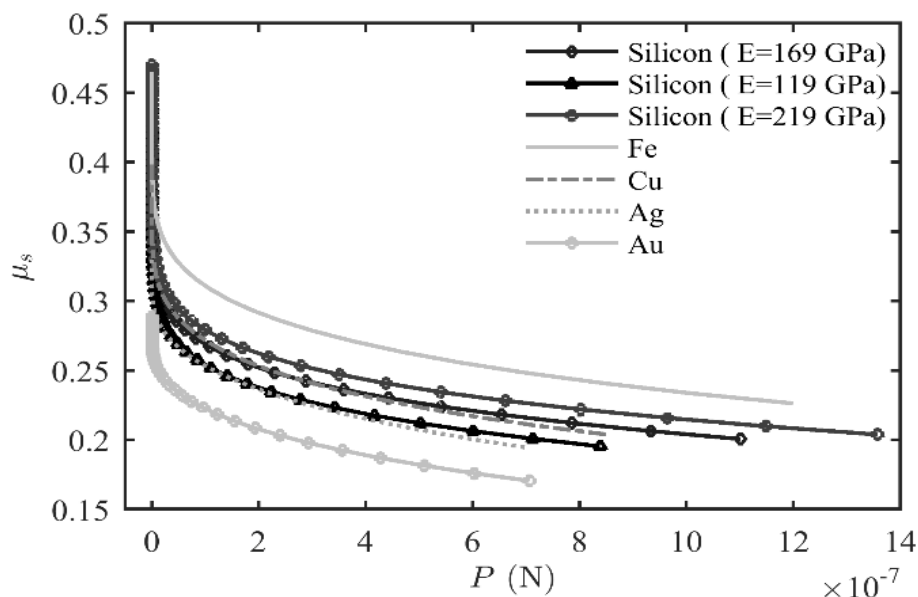


Figure 12 Effect of elasticity modulus and material type on friction coefficient ($\sigma = 1 \text{ nm}$ and $R_r = 50 \text{ nm}$)

Figures (13) and (14) show the changes in normal and frictional forces as a function of distance obtained using the Schwarz, JKR and DMT contact models. They were also compared with the values obtained with the AM (Hertz model). In all diagrams, the forces become smaller with increasing distance. On the other hand, the JKR contact model predicted the most similar results compared to the Schwarz contact model. This is because at small surface separation, the short-range adhesion forces are much larger compared to the long-range forces. It can also be seen in the diagrams of the new modeling based on JKR and Schwarz that at smaller distances of less than 1 nm, the magnitudes of the normal and frictional forces vary by up to 40% compared to the results based on Hertz, which is significant. Moreover, in the HK friction model, the magnitude of the frictional force decreases with increasing contact area. Therefore, the highest friction force is calculated when using the Schwarz contact model.

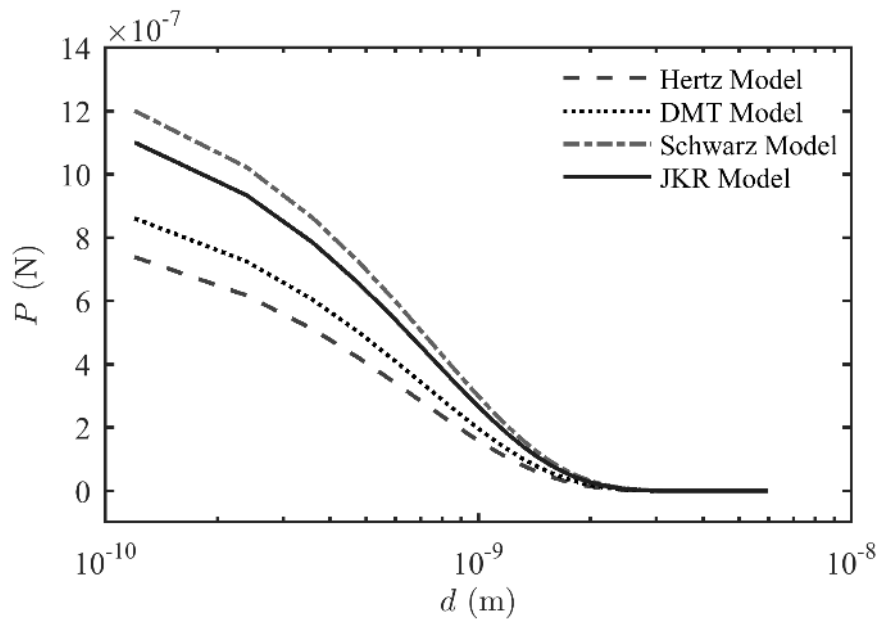


Figure 13 Comparison of normal force in the DAM based on contact models ($\sigma = 1 \text{ nm}$ and $R_r = 50 \text{ nm}$).

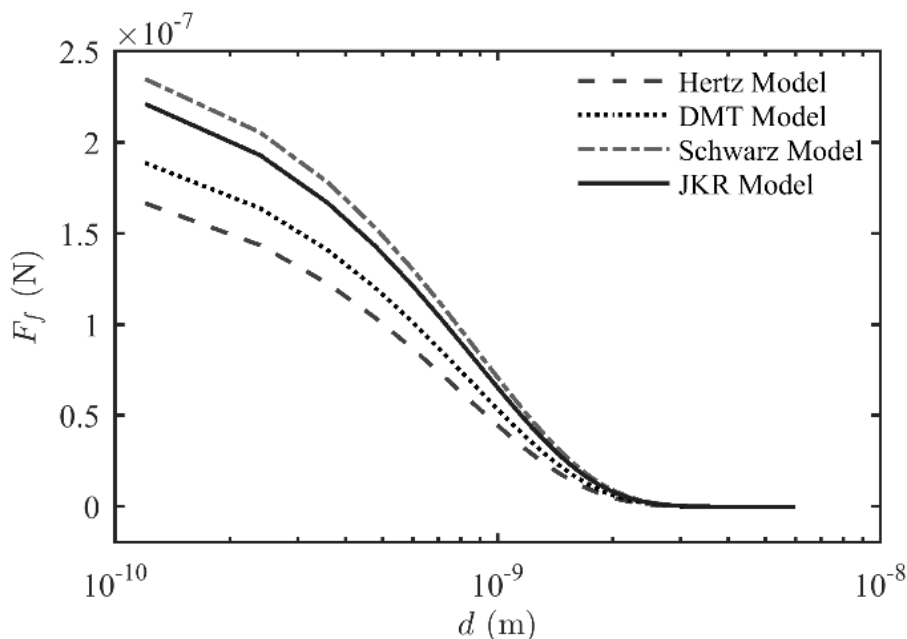


Figure 14 Comparison of friction force in the DAM based on contact models ($\sigma = 1 \text{ nm}$ and $R_r = 50 \text{ nm}$)

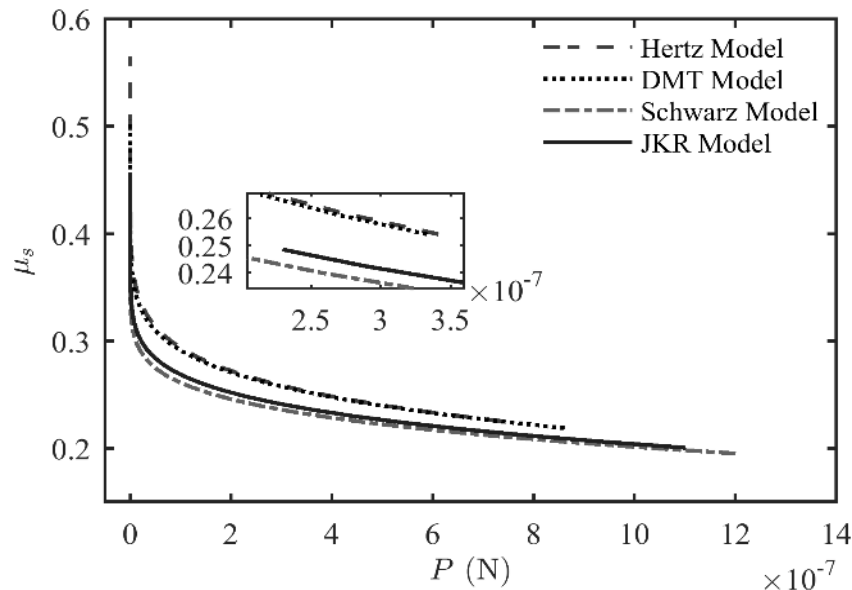


Figure 15 Comparison of friction coefficient in the DAM based on different contact models ($\sigma = 1 \text{ nm}$ and $R_r = 50 \text{ nm}$)

Figure (15) shows that the model based on the Schwarz contact model predicts the lowest friction coefficient. This is due to the fact that the HK friction model predicts lower frictional stress for the contact surfaces with larger radii. Therefore, the Schwarz model predicts the lowest friction force to normal force ratio because it has the largest value for normal force.

The JKR contact model predicts the most similar results compared to the Schwarz contact model. The results obtained for friction behavior were also observed and validated in comparison with previous experimental studies. Moreover, the trend of friction coefficient variation in this study is similar to the existing results [6, 7, 13, 23].

4 Conclusion

In this study, a novel model of friction behavior was developed by integrating the JKR, DMT, and Schwarz contact models with the HK friction model and the GW roughness distribution model. In the simulation section, an analysis of the frictional behavior on contacting surfaces was performed. The main friction-related variables were investigated and evaluated, including normal force, friction force, and friction coefficient. This also included the influence of roughness parameters such as standard deviation of asperity, height and the peak radius of the asperity, and material parameters such as adhesion energy, length of Burgers vector, and elastic modulus on the frictional behavior of rough surfaces. Overall, the results of this study show that the DAM, model based on the JKR contact model predicts higher normal and friction forces than the AM model based on the Hertz contact model. In addition, the model DAM, which is based on the Schwarz model, provides the highest normal and friction forces associated with the lowest friction coefficient. Moreover, the coefficient of friction obtained with the AM model is lower than the corresponding values obtained with the DAM model. In order to investigate the sensitivity of the friction coefficient to the material properties, a comprehensive analysis was performed based on two sets of material parameters. In the first set, which focused on silicon as the base material, the effect of individual parameter variations on the coefficient of friction was evaluated, holding other material parameters constant. In the second set, a range of real materials, including silicon, Fe, Cu, Au, and Ag, were studied in contact with a silicon substrate. Sensitivity analysis showed that the coefficient of friction decreases with increasing adhesion energy, while it increases with greater Burgers vector length and larger elastic modulus. These results are consistent with previous research in this area.

References

- [1] A. H. Dehkordi, N. Montazerin, E. Damangir, and S. M. Rezaei Niya, "Effect of Volute and Rotor Widths on Squirrel Cage Fan Performance and Velocity Profiles," *Iranian Journal of Mechanical Engineering Transactions of the ISME*, vol. 9, no. 2, pp. 80-97, 2020, <https://dorl.net/dor/20.1001.1.16059727.2020.9.2.5.4>.
- [2] H. Haghghat and G. R. Asgari, "A Generalized Upper Bound Solution for Bimetallic Rod Extrusion through Arbitrarily Curved Dies," *Iranian Journal of Mechanical Engineering Transactions of the ISME*, vol. 13, no. 1, pp. 23-35, 2012, <https://dorl.net/dor/20.1001.1.16059727.2012.13.1.2.9>.
- [3] J. Keighobadi, J. Faraji, and S. Rafatnia, "Chaos Control of Atomic force Microscope System Using Nonlinear Model Predictive Control," *Journal of Mechanics*, vol. 33, no. 3, pp. 405-415, 2017, <https://doi.org/10.1017/jmech.2016.89>.
- [4] J. Keighobadi, M. Hosseini-Pishrobat, J. Faraji, A. Oveisi, and T. Nestorović, "Robust Nonlinear Control of Atomic Force Microscope via Immersion and Invariance," *International Journal of Robust and Nonlinear Control*, vol. 29, no. 4, pp. 1031-1050, 2019, <https://doi.org/10.1002/rnc.4421>.
- [5] A. Shahidian, M. R. Mohammadi, and M. Ghasemi, "Numerical Simulation of Blood Flow Mixed with Magnetic Nanoparticles Under the Influence of AC and DC Magnetic Field," *Iranian Journal of Mechanical Engineering Transactions of the ISME*, vol. 15, no. 1, pp. 68-81, 2014, <https://dorl.net/dor/20.1001.1.16059727.2014.15.1.5.6>.
- [6] P. Stempflé and J. Takadom, "Multi-asperity Nanotribological Behavior of Single-Crystal Silicon: Crystallography-induced Anisotropy in Friction and Wear," *Tribology International*, vol. 48, pp. 35-43, 2012, <https://doi.org/10.1016/j.triboint.2011.03.027>.
- [7] A. K. Waghmare and P. Sahoo, "Adhesive Friction at the Contact Between Rough Surfaces Using n-point Asperity Model," *International Journal Engineering Science and Technology*, vol. 18, no. 3, pp. 463-474, 2015, <https://doi.org/10.1016/j.jestch.2015.03.006>.
- [8] Q. Li and K. S. Kim, "Micromechanics of Friction: Effects of Nanometre-scale Roughness," *Royal Society A: Mathematical, Physical and Engineering Science*, vol. 464, no. 2093, pp. 1319-1343, 2008, <https://doi.org/10.1098/rspa.2007.0364>.
- [9] D. Cohen, Y. Kligerman, and I. Etsion, "A Model for Contact and Static Friction of Nominally Flat Rough Surfaces Under Full Stick Contact Condition," *Journal of Tribology*, vol. 130, no. 3, p. 031401, 2008, <https://doi.org/10.1115/1.2908925>.
- [10] J. A. Hurtado and K. S. Kim, "Scale Effects in Friction of Single-asperity Contacts. I. From Concurrent Slip to Single-dislocation-assisted Slip," *Royal Society A: Mathematical, Physical and Engineering Science*, vol. 455, no. 1989, pp. 3363-3384, 1999, <https://doi.org/10.1098/rspa.1999.0455>.
- [11] Y. Dong, A. Vadakkepatt, and A. Martini, "Analytical Models for Atomic Friction," (in English), *Tribol Lett*, vol. 44, no. 3, pp. 367-386, 2011, <https://doi.org/10.1007/s11249-011-9850-2>.

- [12] G. E. Stavroulakis, *Recent Advances in Contact Mechanics*, 4th ed. Berlin Heidelberg: Springer, 2013, pp. 67-84.
- [13] X. S. Tang, Y. C. Loke, P. Lu, S. K. Sinha, and S. J. O'Shea, "Friction Measurement on Free Standing Plates Using Atomic Force Microscopy," *Review of Scientific Instruments*, vol. 84, no. 1, pp. 013702-9, 2013, <https://doi.org/10.1063/1.4773534>.
- [14] K. L. Johnson, *Contact Mechanics*, 1st ed. Cambridge: Cambridge university press, 1987.
- [15] J. A. Hurtado and K. S. Kim, "Scale Effects in Friction of Single-asperity Contacts. II. Multiple-dislocation-cooperated Slip," *Royal Society A: Mathematical, Physical and Engineering Science*, vol. 455, no. 1989, pp. 3385-3400, 1999, <https://doi.org/10.1098/rspa.1999.0456>.
- [16] M. H. Korayem, M. Taheri, and M. Zakeri, "Sensitivity Analysis of Nanoparticles Manipulation Based on Different Friction Models," *Applied surface science*, vol. 258, no. 18, pp. 6713-6722, 2012, <https://doi.org/10.1016/j.apsusc.2011.12.024>.
- [17] D. Maugis, "Adhesion of Spheres: The JKR-DMT Transition Using a Dugdale Model," *Journal of Colloid and Interface Science*, vol. 150, no. 1, pp. 243-269, 1992, [https://doi.org/10.1016/0021-9797\(92\)90285-T](https://doi.org/10.1016/0021-9797(92)90285-T).
- [18] U. D. Schwarz, "A Generalized Analytical Model for the Elastic Deformation of an Adhesive Contact Between a Sphere and a Flat Surface," *Journal of Colloid and Interface Science*, vol. 261, no. 1, pp. 99-106, 2003, [https://doi.org/10.1016/S0021-9797\(03\)00049-3](https://doi.org/10.1016/S0021-9797(03)00049-3).
- [19] P. Spijker, G. Anciaux, and J. F. Molinari, "The Effect of Loading on Surface Roughness at the Atomistic Level," *Computational Mechanics*, vol. 50, no. 3, pp. 273-283, 2012, <https://doi.org/10.1007/s00466-011-0574-9>.
- [20] T. D. Jacobs *et al.*, "The Effect of Atomic-scale Roughness on the Adhesion of Nanoscale Asperities: A Combined Simulation and Experimental Investigation," *Tribol Lett*, vol. 50, no. 1, pp. 81-93, 2013, <https://doi.org/10.1007/s11249-012-0097-3>.
- [21] L. Pin and S. J. O' Shea, "Mechanical Contact Between Rough Surfaces at Low Load," *Journal of Physics D: Applied Physics*, vol. 45, no. 47, pp. 475303-18, 2012, <https://doi.org/10.1088/0022-3727/45/47/475303>.
- [22] V. A. Yastrebov, G. Anciaux, and J. F. Molinari, "From Infinitesimal to Full Contact Between Rough Surfaces: Evolution of the Contact Area," *International Journal of Solids and Structures*, vol. 52, pp. 83-102, 2015, <https://doi.org/10.1016/j.ijsolstr.2014.09.019>.
- [23] C. D. Yeo, R. R. Katta, J. Lee, and A. A. Polycarpou, "Effect of Asperity Interactions on Rough Surface Elastic Contact Behavior: Hard Film on Soft Substrate," *Tribology International*, vol. 43, no. 8, pp. 1438-1448, 2010, <https://doi.org/10.1016/j.triboint.2010.01.021>.
- [24] M. Ciavarella and A. Papangelo, "On the Sensitivity of Adhesion Between Rough Surfaces to Asperity Height Distribution," *Physical Mesomechanics*, vol. 21, no. 1, pp. 59-66, 2018, <https://doi.org/10.1134/S1029959918010083>.

- [25] G. G. Adams, S. Müftü, and N. Mohd Azhar, "A Scale-dependent Model for Multi-Asperity Contact and Friction," *Journal of Tribology*, vol. 125, no. 4, pp. 700-708, 2003, <https://doi.org/10.1115/1.1573232>.
- [26] B. Sista and K. Vemaganti, "Estimation of Statistical Parameters of Rough Surfaces Suitable for Developing Micro-asperity Friction Models," *Wear*, vol. 316, no. 1-2, pp. 6-18, 2014, <https://doi.org/10.1016/j.wear.2014.04.012>.
- [27] J. Yu *et al.*, "Quantitative Investigation on Single-asperity Friction and Wear of Phosphate Laser Glass Against a Spherical AFM Diamond Tip," *Tribology International*, vol. 81, pp. 43-52, 2014, <https://doi.org/10.1016/j.triboint.2014.07.020>.
- [28] P. Lu, L. Yang, and G. Wang, "Studies of Low-loading Micro-slip Contacts on Rough Surfaces with GW Model," *International Journal of Applied Mechanics*, vol. 9, no. 04, p. 1750049, 2017, <https://doi.org/10.1142/S1758825117500491>.
- [29] J. A. Greenwood and J. P. Williamson, "Contact of Nominally Flat Surfaces," *Royal Society A: Mathematical, Physical and Engineering Science*, vol. 295, no. 1442, pp. 300-319, 1966, <https://doi.org/10.1098/rspa.1966.0242>.
- [30] G. A. George and M. Sinan, "Improvements to a Scale-dependent Model for Contact and Friction," *Journal of Physics D: Applied Physics*, vol. 38, no. 9, pp. 1402-1409, 2005, <https://doi.org/10.1088/0022-3727/38/9/012>.
- [31] M. Zakeri and J. Faraji, "Modeling the Adhesion of Spherical Particles on Rough Surfaces at Nanoscale," *International Journal of Adhesion and Adhesives*, vol. 124, p. 103385, 2023, <https://doi.org/10.1016/j.ijadhadh.2023.103385>.
- [32] M. Zakeri, J. Faraji, and M. Kharazmi, "Multipoint Contact Modeling of Nanoparticle Manipulation on Rough Surface," *Journal of Nanoparticle Research*, vol. 18, no. 12, p. 374, 2016, <https://doi.org/10.1007/s11051-016-3639-z>.
- [33] M. Zakeri and J. Faraji, "Modeling of the Rough Spherical Nanoparticles Manipulation on a Substrate Based on the AFM Nanorobot," *Applied Physics A*, vol. 117, no. 4, pp. 1947-1962, 2014, <https://doi.org/10.1007/s00339-014-8668-9>.
- [34] D. F. Parsons, R. B. Walsh, and V. S. Craig, "Surface Forces: Surface Roughness in Theory and Experiment," *The Journal of Chemical Physics*, vol. 140, no. 16, pp. 164701-10, 2014, <https://doi.org/10.1063/1.4871412>.
- [35] M. Zakeri and J. Faraji, "Dynamic Modeling of Nano/Microparticles Displacement in Multi-point Contact Based on the Rumpf Model," (in Persian), *Modares Mechanical Engineering*, vol. 16, no. 8, pp. 120-130, 2016, <https://dorl.net/dor/20.1001.1.10275940.1395.16.8.37.4>.
- [36] A. Fattahi Avati and M. R. Karafi, "Theoretical Study of Effective Parameters in the Friction Reduction by Ultrasonic Vibrations in Solid Surfaces," *Iranian Journal of Mechanical Engineering Transactions of the ISME*, vol. 23, no. 2, pp. 129-144, 2022, <https://doi.org/10.21203/rs.3.rs-1329471/v1>.

Nomenclature

a	Contact radius (m)
\bar{a}	Dimensionless contact radius
a_{DMT}	Contact radius of the DMT model (m)
a_{JKR}	Contact radius of the JKR model (m)
b	Burgers vector length (m)
B	y- intercept of Region 2 of the HK model
d	Separation (m)
\bar{d}	Dimensionless separation
E	Young's modulus (GPa)
E^*	Effective Young's modulus (GPa)
F_f	Friction force (N)
$F_{f\text{total}}$	Total friction force (N)
G	Shear modulus (GPa)
G^*	Effective shear modulus (GPa)
M	Slope of curve in Region 2 of the HK model
n	Number of in contact asperities
N	Total number of asperities
P	External applied force (N)
P_{DMT}	Normal force of the DMT model (N)
P_{JKR}	Normal force of the JKR model (N)
P_H^{JKR}	Equivalent Hertzian force of the JKR model
\bar{P}_n	Dimensionless normal force
R	Radius of sphere (m)
R_r	Radius of asperity curvature (m)
R_s	Effective radius of bodies in contact (m)
z	Asperity height (m)
\bar{z}	Dimensionless asperity height
α	Surface roughness parameter
β	Friction regime parameter
γ	Surface energy coefficient (Jm^{-2})
δ	Indentation depth (m)
μ	Mean value of asperity height
μ_s	Friction coefficient
ν	Poisson's ratio
ρ	Density (kgm^{-3})
σ	Standard deviation of asperity height
τ_1	Transition parameter in the Schwarz model
τ_f	Friction stress (MPa)
$\bar{\tau}_f$	Dimensionless friction stress
φ	Asperity peak distribution probability